



Antiangiogenic evaluation of ZnWO₄ nanoparticles synthesized through microwave-assisted hydrothermal method

Carla Júnia Santos, Daniel Crístian Ferreira Soares, Carolina de Aguiar Ferreira, André Luís Branco de Barros, Armando da Silva Cunha Junior & Francisco Moura Filho

To cite this article: Carla Júnia Santos, Daniel Crístian Ferreira Soares, Carolina de Aguiar Ferreira, André Luís Branco de Barros, Armando da Silva Cunha Junior & Francisco Moura Filho (2018): Antiangiogenic evaluation of ZnWO₄ nanoparticles synthesized through microwave-assisted hydrothermal method, Journal of Drug Targeting, DOI: [10.1080/1061186X.2018.1428810](https://doi.org/10.1080/1061186X.2018.1428810)

To link to this article: <https://doi.org/10.1080/1061186X.2018.1428810>



Accepted author version posted online: 22 Jan 2018.



Submit your article to this journal [↗](#)



Article views: 1



View related articles [↗](#)



View Crossmark data [↗](#)

Antiangiogenic evaluation of ZnWO₄ nanoparticles synthesized through microwave-assisted hydrothermal method

Carla Júnia Santos¹, Daniel Crístian Ferreira Soares^{1*}, Carolina de Aguiar Ferreira², André Luís Branco de Barros³, Armando da Silva Cunha Junior³ and Francisco Moura Filho¹

1- Universidade Federal de Itajubá - Laboratório de Bioengenharia - Rua Irmã Ivone Drumond, 200, Distrito Industrial II, 35903-087 - Itabira, Minas Gerais, Brazil.

2- University of Wisconsin Madison – Department of Biomedical Engineering – Highland Avenue, 1111, Madison, Wisconsin, 53705, USA

3- Universidade Federal de Minas Gerais - Faculdade de Farmácia - Avenida Presidente Antônio Carlos 6627, Pampulha, 31270-901- Belo Horizonte, Minas Gerais, Brazil

*Corresponding author:

soares@unifei.edu.br

Keywords: Zinc tungstate oxide nanoparticles; ZnWO₄ microwave-assisted hydrothermal synthesis; ZnWO₄ antiangiogenic activity; ZnWO₄ cytotoxic evaluation

Abstract

Angiogenesis, the complex process of formation of new blood vessels from pre-existing blood vessels, which involves the participation of several pro and anti-angiogenic factors, is implicated in many physiological and pathological conditions. Nanoparticle-based anti-angiogenic activity at the tumor tissue, harnessed by the Enhanced Permeability and Retention Effect (EPR effect), could potentially become a breakthrough therapy to halt tumor progression. Herein, we evaluate the anti-angiogenic effect of ZnWO₄ nanoparticles (NPs). The nanoparticles were obtained by microwave-assisted hydrothermal synthesis (MAHS) at 120 °C for 60 min and were structurally characterized by X-ray diffraction (XRD) and micro-Raman (MR) spectroscopy. The mean size and polydispersity index were estimated by Zeta potential analysis. The XRD analysis revealed structural organization at a long-range order, with an average crystallite size of around 3,67nm, while MR revealed short-range order for ZnWO₄. The anti-angiogenic potential of zinc tungstate nanoparticles was investigated through the chorioallantoic membrane assay (CAM) using fertilized chicken eggs. We demonstrate, in an unprecedented way, that nanocrystalline ZnWO₄ NPs obtained by MAHS, at low reaction temperatures, showed excellent anti-angiogenic properties even at low concentrations. The ZnWO₄ NPs were further evaluated for its cytotoxicity in vitro.

1. Introduction

Over the last decade, the oncology field has been experiencing a boom in anti-angiogenic based anti-tumoral approaches, since it is well established that tumor growth and metastatic behavior are processes completely dependent of an angiogenic activity that is able to support the growing demands of nutrients and oxygen. Triggered by many chemical mediators produced by tumor cells, the control of the angiogenic process can pose as a breakthrough therapeutic method. However, results obtained from clinical trials have been solely modest [1–3].

The angiogenesis process was discovered two centuries ago by John Hunter who observed that new blood vessel formation was a fundamental stage in tissue expansion and recovery [4]. Upon hypoxia or endothelial cells death, surviving cells in close proximity are triggered to produce and release specific chemical growth factors that, in turn, promotes cell proliferation and stabilization resulting in increased cell division of endothelial cells. Various growth factors have been identified as angiogenic factors such as Transforming Growth Factor (TGF)- α , Basic Fibroblast Growth Factor (bFGF), Alpha-Tumor Necrosis Factor (TNF)- α and mainly the Vascular Endothelial Growth Factor (VEGF). Nowadays, more than 10 approved drugs that either target growth factors directly or their receptors, have been approved for the treatment of various tumors and are currently in use in the clinical settings [5,6].

VEGF, perhaps the most important angiogenic factor of them all, is widely quantified in tumor tissues and has been the preferred target for anti-angiogenic approaches due to its central role in neovascularization. The first VEGF-based therapeutic monoclonal antibody, developed by Ferrara and co-workers in 2003, is known as Bevacizumab and have resulted in important

therapeutic benefits to colon cancer patients [7]. Fourteen years later, several other therapeutic agents, focused on the VEGFA pathway inhibition, can be found in the market, such as Sorafenib[®], Vandetanib[®], and Lenvatinib[®] developed in 2015 for the treatment of refractory thyroid cancer [8–10]. Unfortunately, selective targeting of vasculature instead of the tumor cells themselves still means that all blood vessels in the body are a potential target of these modern drugs and this lack of selectivity for tumor blood vessels has largely limited its use as relevant side effects are observed on epithelial stem and progenitor cells of hematopoietic in the bone marrow [11,12]. In this context, the discovery and development of new anti-angiogenic agents have attracted much interest in the last few years, and some new classes of compounds have been showing promising anti-angiogenic activity, such as metal and oxide nanoparticles. For example, studies conducted by Gurunathan and co-workers showed important anti-angiogenic activity mediated by silver nanoparticles [13]. Huang and co-workers studied the zinc-chelation effects on inhibition of activity, migration and tube formation of human endothelial cells [14]. Cuprous oxide nanoparticles inhibited angiogenesis via down-regulation of VEGFR2 expression according to studies conducted by Song et al. [15].

Of note, nanoparticle-based therapy is a promising approach in cancer due to an effect called Enhanced Permeability and Retention (EPR). EPR effect is based on the fact that tumor vasculature is leaky and circulating NPs can accumulate more in the tumor tissues than in normal tissues. Also, the lymphatic drainage is not efficient at those sites, allowing prolonged retention of these molecules in the targeted tissue [16,17]. In this context, NPs can harness the anatomical differences between normal and tumor tissue, and considering

the role of inorganic nanoparticles in angiogenesis inhibition, in the present study, we investigated the antiangiogenic properties of ZnWO₄ nanoparticles aiming to evaluate this oxide as a potential new anti-angiogenic agent.

2. Experimental procedure

2.1. ZnWO₄ nanoparticles synthesis

ZnWO₄ nanoparticles were prepared through microwave-assisted hydrothermal synthesis (MAHS) as described previously by Yu and co-workers[18], with a few modifications. In brief, ZnCl₂ (Vetec, purity > 99%) and Na₂WO₄ · 2H₂O (Specsol, purity > 99%) were used as precursors in equimolar amounts. Both salts were dissolved in deionized water under constant magnetic stirring to form homogeneous aqueous solutions of 0,1 mol/L concentrations. Zinc chloride solution was then added to the sodium tungstate solution to obtain precursor suspension. The pH of the suspension was adjusted to 9.0 with KOH (1,0 mol/L). The obtained suspension was added into a Teflon container and then exposed to a microwave oven operating at a frequency of 2,45GHz and a power of 800 W at 120°C, 130°C, 140°C and 150°C for 60 min. After cooling, the product was filtered, washed with deionized water (5 x) and absolute ethyl alcohol (1x) (Synth, purity > 99.5%), and dried at ambient temperature.

2.2. Physicochemical characterization

2.2.1 X-ray diffraction (XRD)

Phase identification was conducted by X-ray Diffraction (XRD), using a Rigaku wide-angle SmartLab vertical goniometer applying CuK_α radiation ($\lambda =$

1,54060 nm). The samples were measured in stepscan mode with steps of $0,02^{\circ}2\theta$ and a scan speed of $1.00^{\circ}.S^{-1}$ from 10 to $80^{\circ}2\theta$.

2.2.2 Raman spectroscopy

Raman spectra were performed on Micro Raman spectrometer (HORIBA IHR 320) with a 320nm wavelength coupled with a microscope (OLYMPUS BX41). To obtain the Raman spectra, the samples were placed on a microscope, which is equipped with 10, 20 and 50 \times 440 objectives. The Raman spectra were excited by a solid-state laser producing highly polarized light at 633 nm and collected at a resolution of 2 cm^{-1} and a precision of $\pm 1\text{ cm}^{-1}$ in the range between 100 and 1200 cm^{-1} . Repeated acquisition of the nanoparticles, using the highest magnification (50 \times) were accumulated to improve the signal to noise ratio in the spectra. Spectra were calibrated using the 520.5 cm^{-1} line of a silicon wafer.

2.2.3 Mean size, polydispersity index and zeta potential analyses

The average hydrodynamic size, size distribution and zeta potential were determined using dynamic light scattering and phase analysis light scattering in a Zetasizer Nano-ZS equipped with 40 mW, 633 nm laser (Model ZEN 360, Malvern Instruments Ltd, Malvern, UK).

The mean size and polydispersity index of the ZnWO_4 were evaluated by dynamic light scattering (DLS) at an angle of 90° at 25°C . The zeta potential was determined by DLS associated with electrophoretic mobility, at pH 7.4, and

at an angle of 90°. For the measurements of mean size or polydispersity index and zeta potential, the samples of ZnWO₄ nanoparticles (1 µg.mL⁻¹) were dispersed using purified water ($\cong 120 \pm 20$ uS/cm² of conductivity) and subjected to vigorous shaking in a vortex. After complete homogenization, the samples were kept in specific cuvettes provided by the equipment manufacturer.

2.3 Morphological characterization

The structure of ZnWO₄ nanoparticles was analyzed, after gold sputtering, through Scanning Electron Microscopy (SEM), using a TESCAN VEGA 3 LMU (Czech Republic) scanning electron microscope operated at 5 kV.

2.4 In vitro cytotoxic evaluation

2.4.1 Cell culture

Immortalized HEK-293 cells (ATCC[®] CRL-1573) were thawed and cultivated in a direct heat CO₂ incubator (Thermo-Scientific) with humid atmosphere (CO₂-5%) at a temperature of 37°C using DMEM culture medium supplemented with sodium bicarbonate (3.7g/L), 10% of sterile fetal bovine serum and streptomycin at 1% (v/v). After adequate confluency, approximately 1.0X10⁸ cells were placed in 12-wells plates during 24h for proper adhesion. ZnWO₄ NPs dispersions at 1.0, 10.0 and 20.0 µg/mL were added to the wells. Negative controls were treated with sterile phosphate buffer solution (PBS), and positive controls were treated with DMSO at 0.5% for appropriate evaluation. At 48h post-treatment, the cells were removed from the wells using trypsin-EDTA solution at 0.25% (w/v) followed by culture medium for inactivation. A

suspension of treated cells was added to flow cytometry tubes for analysis. All experiments were carried out in replicates for statistical evaluations.

2.4.2 Flow cytometry analysis

Cytotoxicity activity of ZnWO₄ NPs was evaluated through flow cytometry technique using Fixable Viability Stain[®] 450 kits purchased from BD Biosciences (São Paulo-Brazil). This kit allows the discrimination of viable from non-viable cells using a violet fluorescent stain that contains a dye that reacts with and covalently binds to the cell surface and intracellular amines. Permeable plasma cell membranes, such as those present in necrotic cells, allow for the intracellular diffusion of the violet dye and covalent binding to higher overall concentrations of amines than in non-permeable live cells. The parameters constituted by Side Scattering (SSC), Forward Side Scattering (FSC) and color panel of V450 were used during acquisition until 10,000 events were collected for adequate statistical evaluation. A total of five replicates were analyzed by each tested concentration and the acquired data represents the average of different independent experiments.

Apoptosis detection studies procedure were performed using the PE Annexin V apoptosis detection kit I, purchased from BD Biosciences (São Paulo-Brazil) as independent experiments. HEK-293 cells were treated according to methodology procedures described in 2.4.1. After, the cells were washed with cold PBS and resuspended in 1X binding buffer at a concentration of 1x10⁶ cells/mL. Next, 100 µL of the solution (1x10⁵ cells) was transferred to a 5mL culture tube. Then, added 5 µL of PE annexin and 5 µL 7-AAD (7-amino-

actinomycin), the mixture was gently vortex and incubated for 15 min at room temperature (25°C) in the dark. Finally, 400 µL of binding buffer was added to each tube and the analyzes in the flow cytometry were conducted.

2.5 *In vivo* anti-angiogenic activity evaluation

Chorioallantoic membrane assay (CAM) was used to evaluate the *in vivo* antiangiogenic activity of ZnWO₄ NPs in different concentrations of (1.0, 10.0 e 20.0 µg/mL in 20µL of deionized water). Phosphate-buffered-saline (PBS, pH 7.4) was used as a negative control while Bevacizumab solution at 250 µg/mL (Avastin[®], Produtos Roche Químicos e Farmacêuticos S.A., Brazil) was used as the positive control, both in the same volume as the ZnWO₄ samples (20 µL). All experimental procedure is summarized in Figure 1. 20 fertilized chicken eggs, per group, were transferred into a hatching incubator (Premium Ecologica, Brazil) with 60% of relative humidity and temperature fixed at 37 °C. On day 3 of embryonic development, a circular opening of about 1.0 cm in diameter in the region of the air chamber of the eggshell was made, and the inner shell membrane was removed to expose the CAM. On day 5, the samples were applied over the CAM using filter paper disks aiming to control the correct dosage. On the 7th day of incubation, the CAMs were extracted after the previous fixation with 3.7% formaldehyde for 10 min and analyzed with a stereomicroscope (Leica, model DM4000B, Germany) coupled to a Leica digital CCD camera model DFC 280 (Software Leica Application Suite V 3.3.0, Germany). The obtained images were processed with the program Image J

(version 1.44p; National Institutes of Health, USA) in which the control group was set to 100% for blood vessels quantification.

2.6 Statistical analysis

The antiangiogenic and cytotoxic properties of ZnWO₄ NPs were analyzed by one-way Analysis of Variance (ANOVA) followed by post hoc test when appropriate, through GraphPad Prism® 5.0 Software. The characterization data was analyzed with Origin Pro 8.5 (OriginLab Corporation, Massachusetts, USA) software. Data are expressed as mean ± standard deviation. A P value less than 0.05 was considered statistically significant.

3. Results and discussion

3.1. ZnWO₄ nanoparticles synthesis

ZnWO₄ NPs were successfully synthesized through MAHS, in which a very thin white powder was obtained, with good dispersion stability in water (Figure 2). Due to its unique physical and chemical properties, several studies have reported the use of ZnWO₄ NPs in the catalysis, optical and electronic fields. However, biological applications of these NPs are currently scarce [19,20] and remain unexplored.

The pioneering work developed by Gedye et al. [21] and Giguere et al. [22], which reported, through microwave radiation methods, a reduction of time and temperature during synthesis, led to an increased interest of applying this technique to the synthesis of organic compounds, including nanoparticles.

The higher reaction speed of hydrothermal systems coupled to microwave radiation can be explained by two main effects, so-called thermal and non-thermal or specific [23,24] effects. The thermal effect, also called dielectric

heating, is the result of the dipolar polarization from the dipole-dipole interactions of the material and the electromagnetic field, which depends exclusively on the dielectric properties of the material [23,25–29]. The non-thermal effect, on the other hand, is characterized by the ability of the microwave radiation to alter the thermodynamic properties of the reaction system, either by an enthalpic effect as a result of the free energy storage of microwave or vibrational energy of a molecule or functional group or an entropic effect due to the alignment of the molecules caused by the energy of microwave radiation. Altogether, these effects create a new reaction pathway with lower activation energy [30–32]. Besides these increase in reaction speed, MAHS methodology also allows the possibility of obtaining particles in the nanoscale, with high purity and crystallinity [33–36] and was the method of choice for our synthesis step.

In this work, semi-crystalline ceramic powders of ZnWO_4 nanoparticles were successfully obtained at 120°C and 130°C through MAHS, for 60 min. However, fully crystalline ZnWO_4 NPs were obtained using a temperature of 140°C and 150 °C. All results were confirmed by XRD technique.

3.2. Physicochemical characterization

3.2.1. XRD

The long-range structural order of the nanoparticle crystals was evaluated by XRD patterns analysis, and the results are shown in Figure 3. It was possible to observe the majority of the peaks expected for the hydrothermally synthesized ZnWO_4 NPs, in accordance with standard data (DB card number 01-089-0447, PDXL, Rigaku) described for the monoclinic

sanmartinite phase of ZnWO_4 with wolframite structure (C2h point symmetry and P2c space group) suggesting the formation of a solid monocrystalline suspension. After microwave irradiation at 120°C for 60 minutes, ZnO_6 clusters and octahedral WO_6 could be seen (Figure 1)., Using Scherer's equation, based on full width at half maximum (FWHM) of direction (111), the average crystallite size of the sample was estimated to be approximately 3,67nm.

The XRD patterns of ZnWO_4 nanoparticles obtained at different temperatures are shown in Figure 4. All the detected peaks are indexed to ZnWO_4 NPs synthesized at 140°C . With the increase in temperature, it was possible to observe higher intensity and diminished total width of the peaks, indicating an increase not only in crystallinity but also in size, which was in agreement with the average size values of crystallite obtained through the Scherrer's equation (table 1). Thus, in comparison with the conventional hydrothermal pathway, the use of microwave radiation results in a product with better crystallinity even within a shorter treatment time. This faster crystallization kinetics clearly states the advantages of using microwave radiation for nanoparticle synthesis.

Several studies have previously demonstrated the efficacy of microwave-assisted hydrothermal synthesis to obtain oxides and mixed-oxides nanoparticles [33–37], but the use of MAHS for the preparation of tungstate nanoparticles remained unexplored. In this work, ZnWO_4 nanoparticles were successfully obtained through described micro-wave assisted methodology.

3.2.2 Raman spectroscopy

Raman spectroscopy is an excellent technique that allows the observation of structural defects as well as the short and medium-range order in the crystalline organization. Raman spectra of ZnWO_4 nanoparticles are presented in Figure 5, which revealed crystals of short-range order even before microwave irradiation. MR analysis showed the initial formation of ZnO_6 and WO_6 octahedra. Group theory analysis for wolframite-type ZnWO_4 NPs predicts 36 lattice modes, in which 18 even vibrations ($8A_g + 10B_g$) are Raman active. The monoclinic wolframite-type structure of ZnWO_4 is formed by interconnected zigzag chains of distorted ZnO_6 and WO_6 octahedra, running parallel to the z-axis. As indicated in Figure 5, the Raman peaks of ZnWO_4 NPs, obtained by MAHS, at 218, 347, 415, 798, and 902cm^{-1} areas signable to the internal vibrations of the WO_6 octahedra of ZnWO_4 .

Although the Raman spectra of samples synthesized at low temperature do not show all vibrational modes expected, such as samples annealing at high temperatures, the main line at 902cm^{-1} , which corresponds to the stretching W-O mode, was observed. Raman signals observed in this work are close to those found by Basiev et al. [38] for BaWO_4 nanoparticles when analyzed at higher temperatures. In that study, two vibrational modes between 750 and 950cm^{-1} for were determined in temperatures lower than 1770K while in temperatures higher than 1770K the authors observed two bands close to 800cm^{-1} , attributed to the phase transition of tungstates.

XRD patterns revealed ZnO_6 clusters and WO_6 octahedra formation after MAHS at 120°C . However, MR analysis, which is much more sensitive than XRD, showed the presence of clusters in the precipitate (data not shown).

Kloprogge et al. [39] found that single-phase synthesis of metal tungstates can be successfully performed by MAHS. However, the crystallinity of the scheelite minerals group is higher than that of the wolframite minerals group using the same synthesis conditions.

Similarly, Kalinko and Kuzmin [40] demonstrated that the Raman spectra of ZnWO_4 NPs significantly change according to the synthesis temperature. The authors rationalized that the Raman lines of ZnWO_4 are broadened, at low annealing temperature, due to a reduction in size and dispersion of the crystallites. That affirmation can be further confirmed in this study since XRD results revealed an average crystallite size of around 10nm.

3.2.3. Average size, polydispersity index and zeta potential analyses

According to photon correlation spectroscopy analysis, ZnWO_4 NPs presented a mean hydrodynamic diameter of 349.98 ± 10.29 nm. In addition, analyzing its overall distribution by DLS (Table 2), it could be observed that approximately 42% of the nanoparticles were smaller than 300 nm. The polydispersity index was found to be 0.580 ± 0.17 .

The zeta potential of ZnWO_4 nanoparticles had a value of -17.5mV and is presented in Table 3. In accordance to previously published report by LI et al., (2014) and WANG et al., (2017), [41,42] the negative zeta potential found for ZnWO_4 nanoparticles found can be justified by the negative charge present in the WO_6 and ZnO_6 clusters, consistent with data obtained from XRD and Raman analysis. It is well known that nanoparticles can have different pharmacokinetic behavior and overall biodistribution, depending on its size, shape and zeta potential [43]. As a consequence, these physicochemical

properties will result in different uptake by target cells as well as different therapeutic efficacy and toxicity. Zeta potential (ξ), which refers to the net charge on a surface of a particle, has been shown to affect nanoparticle internalization into different cell lines, in which a negative value ($\xi \leq 10\text{mV}$), for example, promoted strong uptake by the reticuloendothelial cells [44]. Herein, ZnWO_4 nanoparticles exhibited a relatively high negative net charge that could potentially improve efficient uptake by cells. Many researchers have demonstrated that the average diameter of nanoparticles has influenced biodistribution studies. Nanoparticles of larger than 300nm and smaller than 70nm are rapidly cleared from circulation by mononuclear phagocyte system (MPS) cells [45]. However, some strategies can be used to decreased nanoparticles recognition by immune cells, thereby increasing the half-life of their circulation in the blood, such as surface decoration with hydrophilic molecules to reduce serum protein binding through a process of steric hindrance [43].

3.3. Morphological characterization

ZnWO_4 nanoparticles were evaluated by Scanning Electron Microscopy. Figure 6 A, B and C micrographs, obtained with magnifications at 10.000, 20.000 and 50.000 X respectively, revealed groups of agglomerated spherical and nanometric particles, in accordance to the crystallite size values obtained by the Scherrer's equation (table 1) and previously published papers [46–50].

ZnWO_4 nanoparticles of different shapes have been microwave assisted hydrothermally synthesized. He et al. [19] synthesized ZnWO_4 as nanosheets, while others have produced ZnWO_4 nanorods [47,50]. Factors such as the pH

of the precursor solution and the total time of synthesis have been shown to affect the final ZnWO₄ shape. pH also influences the resulted shape of ZnWO₄ nanoparticles synthesized by the conventional hydrothermal route, in which an acidic pH is preferable for the formation of spherical particles during longer synthesis times (6h and 12h) while for shorter periods, basic pH values are favorable [47,49,50].

3.4. In vitro cytotoxic evaluation

The in vitro cytotoxicity profile of ZnWO₄ nanoparticles was investigated through Flow Cytometry using a Fixable Viability Stain[®] 450 kits, different concentrations (1.0, 10.0 e 20.0 µg/mL) of NPs in immortalized HEK-293 cells. This investigation aimed at evaluating the toxicity potential of the nanostructured material in a healthy human cell line. Negative and positive controls were constituted by saline solution (NaCl 0.9 % w/v) and DMSO 0.5%, respectively. A significant percentage of viable cells (99.29 %) was observed in cells treated with negative control while a very low viability (1%) of cells belonging to the group treated with 0.5% DMSO solution was found.

The results of cytotoxicity evaluation of the group treated with 1.0 µg/mL of ZnWO₄ NPs are presented in Figure 7. In Fig. 7A, the parameters FSC-H versus V450-A (viable fixable stain) are presented in which two different cells populations, regarding size, are seen, characterized for elevated values for FSC. The population with high emissions in V450 parameter (gate in purple color) was identified as dead cells (19.59%), while the other population of cells reached a percentage value of 74.30 (Fig. 7B), attributed to living cells (blue

gate). V450 versus SSC parameters are presented in Figure 7D. It was possible to observe very well-defined populations regarding dead and live cells (purple and blue, respectively). Live cells displayed a significant distribution in terms of internal complexity, which was attributed to ZnWO₄ nanoparticles internalization without loss of membrane integrity. In contrast, for the group of dead cells, two populations could be identified with different values of SSC that possibly indicate distinct mechanisms of cells death. A histogram comparing emissions in 450 nm of the group treated with the nanoparticles (in black) with that of the negative control (in red) is presented in Figure 7C. Samples treated with tungstate nanoparticles presented significantly higher values of emissions as well as similar population distributions, further confirming data determined in SSC vs. V-450 graph.

The results of the cytotoxicity study using a higher concentration of nanoparticles (10.0 µg/mL) are presented in Figure 8. Interestingly, the 10-fold increase in concentration did not significantly change the behavior observed previously. Even though cellular content release happened, there was still an important reduction in the percentage of dead cells that reached 14.81% (Fig. 8B; $p < 0.1$). In addition, cell survival level was at 82.80% and was not significantly different than that found in cells treated with 1.0 µg/mL of NPs or that found for the negative control group. In Fig. 8C, a histogram comparing the results of cells treated with the samples at 10.0 µg/mL and controls confirmed the wide distribution (emissions of 450 nm) plotted in SSC vs. V-450 graph (Figure 8D).

In a similar manner, the results observed in the cells treated with 20 µg/mL of NPs are plotted in Figure 9. Importantly, a different behavior was

found when compared to the cells treated with the other two lower concentrations. In the graph of FSC vs. V-450, presented in Fig. 9A, two well-defined populations, corresponding separately to dead cells and live cells, were observed. A significant reduction in cell viability was present and can be associated with a dose-dependent toxicity caused by ZnWO₄ nanoparticles. Similar values were encountered in V-450 vs. SSC graph in which distinct populations of live and dead cells could be identified.

Altogether, our results demonstrate that the ZnWO₄ nanoparticles presented cytotoxic effect in HEK cells at the concentration of 20.0 µg/mL. However they were non-cytotoxic at 1.0 and 10.0 µg/mL. As these nanomaterials are almost unexplored regarding their biological properties, to the best of our knowledge, no other data on their cytotoxicity could be found, and additional studies still need to be conducted for the better understanding of the cytotoxic effect mechanism. Extrapolating, literature data have shown cytotoxic effects for other inorganic nanoparticles in cell cultures. Danielsen et al. [51], for example, demonstrated that ZnO and Ag nanoparticles were highly cytotoxic in human cell cultures of monocytes and endothelial cells, wherein ZnO nanoparticles were most toxic for endothelial cells, whereas Ag NPs were most toxic for the THP-1 monocytic cells. In another study, Yin et al. [52] showed that cytotoxic effect of Ag nanoparticles was dose-dependent when tested in rat cerebellum granule cells.

Assays using the PE Annexin V apoptosis detection kit were conducted in HEK-293 cells and the results are presented in Figure 10. Low percentages of apoptotic process were determined for cells treated with ZnWO₄ at 1.0, 10.0 and 20.0 µg/mL (14.71 ± 6.18; 7.07 ± 3.01 and 10.01 ± 1.49, respectively).

These cells were considered primarily PE-Annexin V and 7-AAD negative since the negative controls (non-treated HEK-293 cells) reached values of 26.12 ± 4.45 % and were considered as basal apoptosis. Thus, even under different concentrations of ZnWO_4 , no statistically significant differences were observed in apoptosis levels, indicating low toxicity profile of nanoparticles on the HEK-293 cells. These results are in accordance with cytotoxicity test performed previously determined. Additional tests using tumor cells line can be relevant to evaluate the potential antitumor activity of these nanoparticles.

3.5. *In vivo* anti-angiogenic activity evaluation

The percentage of blood vessels remaining in the CAM after application of ZnWO_4 dispersion and saline (NC) are shown in Figure 11.

The mean percentage of blood vessels remaining in the CAM after application of ZnWO_4 with concentrations of 1,0, 10,0 e 20,0 $\mu\text{g/mL}$ (55.59 ± 5.84 , 65.36 ± 3.89 , 67.91 ± 10.24 , respectively) were significantly lower than the ones from the NC group, set as 100% ($p < 0.05$) (Figure 11B). These results demonstrate, thus, that ZnWO_4 NPs inhibited angiogenesis *in vivo*, that is, with the absence of formation of new blood vessels from pre-existing blood vessels (Figure 11A). There was no significant difference between the percentage of blood vessels in CAM incubated within the three treated groups (Figure 11B).

In the last decades, many studies have unveiled that pathological angiogenesis directly or indirectly participates in the pathogenesis, symptoms and even death of a group of diseases called angiogenesis-dependent diseases, including cancer, autoimmune diseases, atherosclerosis and macular degeneration [53,54]. Thus, the interest of researchers in the development and

discovery of drugs with pro or anti-angiogenic potential as a strategy for the treatment of the above diseases have raised, primarily focusing on cancer, due to the high morbidity and mortality associated to this disease.

The results of the present study suggest an anti-angiogenic effect of ZnWO_4 nanoparticles, such as previous reports that indicate antiangiogenic effects of silver and gold nanoparticles [13,55]. Imai et al. [56] demonstrated the antiangiogenic effect in a concentration-dependent manner, of zinc oxide nanoparticles. However, those results were inconclusive since the authors also observed a significant cytotoxic effect of the material in dermis cell culture. Herein, in contrast, it is noteworthy to mention that we observed an antiangiogenic effect even at lower nanoparticle concentrations, which did not promote a toxic effect, facilitating further studies in animal models of angiogenesis. We, therefore, strongly believe that studies related to anti-angiogenic properties should always be accompanied by cytotoxicity assays to exclude the possibility that the anti-angiogenic effect is a mere correlation to the cytotoxic effect of the material.

4. Conclusion

In this study, ZnWO_4 nanoparticles were successfully obtained through microwave-assisted hydrothermal synthesis. The Raman spectroscopy and X-ray diffractometry data revealed compounds with important structural organization in the long and short-range order, while the morphological analyzes indicate that the zinc tungstate nanoparticles have a spherical shape in nanometric scale. These nanoparticles presented cytotoxic activity against HEK cells in a concentration-dependent manner, and the anti-angiogenic

properties of the ZnWO₄ nanoparticles are herein described for the first time. Importantly, the nanoparticles presented anti-angiogenic activity even at lower concentrations. Since ZnWO₄ nanoparticles obtained by MAHS methodology is still poorly explored in the literature, additional in vitro and in vivo studies should be conducted with the aim of assessing the mechanism of anti-angiogenic action of these nanoparticles. Future studies should consider testing ZnWO₄ nanoparticles with reduced mean diameter (below than 200 in order to maximize the EPR effect) aiming to compare the antiangiogenic behavior from different nanoparticles sizes and also include cytotoxicity evaluation of the material in different cell lines such as endothelial cells, which may allow better correlation between the anti-angiogenic effect and the cytotoxic effect.

Acknowledgments

The authors would like to thank Coordenação de Aperfeiçoamento de Pessoal de Nível Superior (CAPES), Conselho Nacional de Desenvolvimento Científico e Tecnológico (CNPq), Fundação de Amparo a Pesquisa do Estado de Minas Gerais (FAPEMIG) and Rede Mineira de Química for their financial support.

Conflict of Interests

The authors report no conflict of interests.

References

- [1] B. Rashidi, M. Malekzadeh, M. Goodarzi, A. Masoudifar, H. Mirzaei, Green tea and its anti-angiogenesis effects, *Biomed. Pharmacother.* 89 (2017) 949–956. doi:10.1016/j.biopha.2017.01.161.
- [2] J. Folkman, Angiogenesis in cancer, vascular, rheumatoid and other disease., *Nat. Med.* 1 (1995) 27–31. <http://www.ncbi.nlm.nih.gov/pubmed/7584949> (accessed September 21, 2016).
- [3] A.P. Hall, The role of angiogenesis in cancer, *Comp. Clin. Path.* 13 (2005) 95–99. doi:10.1007/s00580-004-0533-3.
- [4] J.A. Stephenson, J.C. Goddard, O. Al-Taan, A.R. Dennison, B. Morgan, Tumour Angiogenesis: A Growth Area—From John Hunter to Judah Folkman and Beyond, *J. Cancer Res.* 2013 (2013) 1–6. doi:10.1155/2013/895019.
- [5] N. Nishida, H. Yano, T. Nishida, T. Kamura, M. Kojiro, Angiogenesis in cancer., *Vasc. Health Risk Manag.* 2 (2006) 213–9. <http://www.ncbi.nlm.nih.gov/pubmed/17326328> (accessed July 10, 2017).
- [6] W.-H. Yang, J. Xu, J.-B. Mu, J. Xie, Revision of the concept of anti-angiogenesis and its applications in tumor treatment, *Chronic Dis. Transl. Med.* 3 (2017) 33–40. doi:10.1016/j.cdtm.2017.01.002.
- [7] N. Ferrara, K.J. Hillan, H.-P. Gerber, W. Novotny, Case history: Discovery and development of bevacizumab, an anti-VEGF antibody for treating cancer, *Nat. Rev. Drug Discov.* 3 (2004) 391–400. doi:10.1038/nrd1381.
- [8] J.E. Frampton, Lenvatinib: A Review in Refractory Thyroid Cancer, *Target. Oncol.* 11 (2016) 115–122. doi:10.1007/s11523-015-0416-3.
- [9] L. Xie, T. Ji, W. Guo, Anti-angiogenesis target therapy for advanced osteosarcoma (Review), *Oncol. Rep.* (2017). doi:10.3892/or.2017.5735.
- [10] J. Krajewska, T. Gawlik, B. Jarzab, Advances in small molecule therapy for treating metastatic thyroid cancer, *Expert Opin. Pharmacother.* (2017) 1–12. doi:10.1080/14656566.2017.1340939.
- [11] C.R. Schlieve, S.G. Mojica, K.A. Holoyda, X. Hou, K.L. Fowler, T.C. Grikscheit, Vascular Endothelial Growth Factor (VEGF) Bioavailability Regulates Angiogenesis and Intestinal Stem and Progenitor Cell Proliferation during Postnatal Small Intestinal Development, *PLoS One.* 11 (2016) e0151396. doi:10.1371/journal.pone.0151396.
- [12] R.K. O'Donnell, B. Falcon, J. Hanson, W.E. Goldstein, C. Perruzzi, S. Raffii, W.C. Aird, L.E. Benjamin, VEGF-A/VEGFR Inhibition Restores Hematopoietic Homeostasis in the Bone Marrow and Attenuates Tumor Growth., *Cancer Res.* 76 (2016) 517–24. doi:10.1158/0008-5472.CAN-14-3023.

- [13] S. Gurunathan, K.J. Lee, K. Kalishwaralal, S. Sheikpranbabu, R. Vaidyanathan, S.H. Eom, Antiangiogenic properties of silver nanoparticles, *Biomaterials*. 30 (2009) 6341–6350. doi:10.1016/j.biomaterials.2009.08.008.
- [14] S.-T. Huang, R.-C. Yang, H.-T. Wu, C.-N. Wang, J.-H.S. Pang, Zinc-chelation contributes to the anti-angiogenic effect of ellagic acid on inhibiting MMP-2 activity, cell migration and tube formation., *PLoS One*. 6 (2011) e18986. doi:10.1371/journal.pone.0018986.
- [15] H. Song, W. Wang, P. Zhao, Z. Qi, S. Zhao, A. Noël, D. Mottet, V. Castronovo, A. Bellahcène, M. Liu, Z. Yi, J.A. Bankson, J.N. Myers, S.Y. Lai, M.L. Lung, Cuprous oxide nanoparticles inhibit angiogenesis via down regulation of VEGFR2 expression, *Nanoscale*. 6 (2014) 3206. doi:10.1039/c3nr04363k.
- [16] I.A. Khawar, J.H. Kim, H.-J. Kuh, Improving drug delivery to solid tumors: Priming the tumor microenvironment, *J. Control. Release*. 201 (2015) 78–89. doi:10.1016/j.jconrel.2014.12.018.
- [17] D. Peer, J.M. Karp, S. Hong, O.C. Farokhzad, R. Margalit, R. Langer, Nanocarriers as an emerging platform for cancer therapy, *Nat. Nanotechnol*. 2 (2007) 751–760. doi:10.1038/nnano.2007.387.
- [18] S.-H. Yu, B. Liu, M.-S. Mo, J.-H. Huang, X.-M. Liu, Y.-T. Qian, General Synthesis of Single-Crystal Tungstate Nanorods/Nanowires: A Facile, Low-Temperature Solution Approach, *Adv. Funct. Mater*. 13 (2003) 639–647. doi:10.1002/adfm.200304373.
- [19] G. He, H. Fan, L. Ma, K. Wang, D. Ding, C. Liu, Z. Wang, Synthesis, characterization and optical properties of nanostructured ZnWO₄, *Mater. Sci. Semicond. Process*. 41 (2016) 404–410. doi:10.1016/j.mssp.2015.09.025.
- [20] R.D. Kumar, Y. Andou, S. Karuppuchamy, Synthesis and characterization of nanostructured Ni-WO₃ and NiWO₄ for supercapacitor applications, *J. Alloys Compd*. 654 (2016) 349–356. doi:10.1016/j.jallcom.2015.09.106.
- [21] R. Gedye, F. Smith, K. Westaway, H. Ali, L. Baldisera, L. Laberge, J. Rousell, The use of microwave ovens for rapid organic synthesis, *Tetrahedron Lett*. 27 (1986) 279–282. doi:10.1016/S0040-4039(00)83996-9.
- [22] R.J. Giguere, T.L. Bray, S.M. Duncan, G. Majetich, Application of commercial microwave ovens to organic synthesis., *Tetrahedron Lett*. 27 (1986) 4945–4948. doi:10.1016/S0040-4039(00)85103-5.
- [23] L. Perreux, A. Loupy, A tentative rationalization of microwave effects in organic synthesis according to the reaction medium, and mechanistic considerations, *Tetrahedron*. 57 (2001) 9199–9223. doi:10.1016/S0040-4020(01)00905-X.
- [24] P. Lidström, J. Tierney, B. Wathey, J. Westman, Microwave assisted organic

- synthesis—a review, *Tetrahedron*. 57 (2001) 9225–9283. doi:10.1016/S0040-4020(01)00906-1.
- [25] J. Anwar, U. Shafique, Waheed-uz-Zaman, R. Rehman, M. Salman, A. Dar, J.M. Anzano, U. Ashraf, S. Ashraf, Microwave chemistry: Effect of ions on dielectric heating in microwave ovens, *Arab. J. Chem.* 8 (2015) 100–104. doi:10.1016/j.arabjc.2011.01.014.
- [26] C. Gabriel, S. Gabriel, E. H. Grant, E. H. Grant, B. S. J. Halstead, D. Michael P. Mingos, Dielectric parameters relevant to microwave dielectric heating, *Chem. Soc. Rev.* 27 (1998) 213. doi:10.1039/a827213z.
- [27] C.O. Kappe, Controlled Microwave Heating in Modern Organic Synthesis, *Angew. Chemie Int. Ed.* 43 (2004) 6250–6284. doi:10.1002/anie.200400655.
- [28] V. Polshettiwar, R.S. Varma, Microwave-Assisted Organic Synthesis and Transformations using Benign Reaction Media, *Acc. Chem. Res.* 41 (2008) 629–639. doi:10.1021/ar700238s.
- [29] R.S.V. and, D. Kumar, Microwave-Accelerated Solvent-Free Synthesis of Thioketones, Thiolactones, Thioamides, Thionoesters, and Thioflavonoids, (1999). doi:10.1021/OL990629A.
- [30] M. Antonia Herrero, and Jennifer M. Kremsner, C.O. Kappe*, Nonthermal Microwave Effects Revisited: On the Importance of Internal Temperature Monitoring and Agitation in Microwave Chemistry, (2007). doi:10.1021/JO7022697.
- [31] A.R. Katritzky, Microwave-assisted heterocyclic synthesis, *Arkivoc.* 2003 (2003) 68–86. doi:10.3998/ark.5550190.0004.d09.
- [32] H. Naeimi, A. Raeisi, M. Moradian, Microwave assisted chemistry: A rapid and regioselective route for direct ortho -acylation of phenols and naphthols by methanesulfonic acid as catalyst, *Arab. J. Chem.* 10 (2017) S2723–S2728. doi:10.1016/j.arabjc.2013.10.017.
- [33] A.C. Cabral, L.S. Cavalcante, R.C. Deus, E. Longo, A.Z. Simões, F. Moura, Photoluminescence properties of praseodymium doped cerium oxide nanocrystals, *Ceram. Int.* 40 (2014) 4445–4453. doi:10.1016/j.ceramint.2013.08.117.
- [34] Y.V.B. De Santana, J.E.C. Gomes, L. Matos, G.H. Cruvinel, A. Perrin, C. Perrin, J. Andrès, J.A. Varela, E. Longo, Silver Molybdate and Silver Tungstate Nanocomposites with Enhanced Photoluminescence, *Nanomater. Nanotechnol.* 4 (2014) 22. doi:10.5772/58923.
- [35] I.M. Pinatti, T.M. Mazzo, R.F. Gonçalves, J.A. Varela, E. Longo, I.L.V. Rosa, CaTiO₃ and Ca_{1–3x}Sm_xTiO₃: Photoluminescence and morphology as a result of

- Hydrothermal Microwave Methodology, *Ceram. Int.* 42 (2016) 1352–1360. doi:10.1016/j.ceramint.2015.09.074.
- [36] L.S.R. Rocha, C.R. Foschini, C.C. Silva, E. Longo, A.Z. Simões, Novel ozone gas sensor based on ZnO nanostructures grown by the microwave-assisted hydrothermal route, *Ceram. Int.* 42 (2016) 4539–4545. doi:10.1016/j.ceramint.2015.11.145.
- [37] L.F. da Silva, A.C. Catto, W. Avansi, L.S. Cavalcante, V.R. Mastelaro, J. Andrés, K. Aguir, E. Longo, Acetone gas sensor based on α -Ag₂WO₄ nanorods obtained via a microwave-assisted hydrothermal route, *J. Alloys Compd.* 683 (2016) 186–190. doi:10.1016/j.jallcom.2016.05.078.
- [38] T.. Basiev, A.. Sobol, Y.. Voronko, P.. Zverev, Spontaneous Raman spectroscopy of tungstate and molybdate crystals for Raman lasers, *Opt. Mater. (Amst)*. 15 (2000) 205–216. doi:10.1016/S0925-3467(00)00037-9.
- [39] J.T. Klopogge, M.L. Weier, L. V. Duong, R.L. Frost, Microwave-assisted synthesis and characterisation of divalent metal tungstate nanocrystalline minerals: ferberite, hübnerite, sanmartinite, scheelite and stolzite, *Mater. Chem. Phys.* 88 (2004) 438–443. doi:10.1016/j.matchemphys.2004.08.013.
- [40] A. Kalinko, A. Kuzmin, Raman and photoluminescence spectroscopy of zinc tungstate powders, *J. Lumin.* 129 (2009) 1144–1147. doi:10.1016/j.jlumin.2009.05.010.
- [41] K. Li, J. Xue, Y. Zhang, H. Wei, Y. Liu, C. Dong, ZnWO₄ nanorods decorated with Ag/AgBr nanoparticles as highly efficient visible-light-responsive photocatalyst for dye AR18 photodegradation, *Appl. Surf. Sci.* 320 (2014) 1–9. doi:10.1016/j.apsusc.2014.09.060.
- [42] Q. Wang, Y. Shi, T. Niu, J. He, H. She, B. Su, Preparing ZnWO₄–CdS composite with excellent visible light photocatalytic activity under mild conditions, *J. Sol-Gel Sci. Technol.* (2017). doi:10.1007/s10971-017-4434-8.
- [43] M.J. Ernsting, M. Murakami, A. Roy, S.D. Li, Factors controlling the pharmacokinetics, biodistribution and intratumoral penetration of nanoparticles, *J. Control. Release.* 172 (2013) 782–794. doi:10.1016/j.jconrel.2013.09.013.
- [44] H. Zhang, K. Zhou, Z. Li, S. Huang, Plate-like hydroxyapatite nanoparticles synthesized by the hydrothermal method, *J. Phys. Chem. Solids.* 70 (2009) 243–248. doi:10.1016/j.jpcs.2008.10.011.
- [45] R. Gref, Y. Minamitake, M.T. Peracchia, V. Trubetskoy, V. Torchilin, R. Langer, Biodegradable long-circulating polymeric nanospheres., *Science.* 263 (1994) 1600–3. <http://www.ncbi.nlm.nih.gov/pubmed/8128245> (accessed December 28, 2017).

- [46] J. Bi, L. Wu, Z. Li, Z. Ding, X. Wang, X. Fu, A facile microwave solvothermal process to synthesize ZnWO₄ nanoparticles, *J. Alloys Compd.* 480 (2009) 684–688. doi:10.1016/j.jallcom.2009.02.029.
- [47] S.-J. Chen, J.-H. Zhou, X.-T. Chen, J. Li, L.-H. Li, J.-M. Hong, Z. Xue, X.-Z. You, Fabrication of nanocrystalline ZnWO₄ with different morphologies and sizes via hydrothermal route, *Chem. Phys. Lett.* 375 (2003) 185–190. doi:10.1016/S0009-2614(03)00878-9.
- [48] C. Li, Y. Liang, J. Mao, L. Ling, Z. Cui, X. Yang, S. Zhu, Z. Li, Enhancement of gas-sensing abilities in p-type ZnWO₄ by local modification of Pt nanoparticles, *Anal. Chim. Acta.* 927 (2016) 107–116. doi:10.1016/j.aca.2016.04.050.
- [49] N. Van Minh, N.M. Hung, D.T. Xuan Thao, M. Roeffaers, J. Hofkens, Structural and Optical Properties of ZnWO₄:Er³⁺ Crystals, *J. Spectrosc.* 2013 (2013) 1–5. doi:10.1155/2013/424185.
- [50] Y. Zhai, M. Wang, Q. Zhao, J. Yu, X. Li, Fabrication and Luminescent properties of ZnWO₄:Eu³⁺, Dy³⁺ white light-emitting phosphors, *J. Lumin.* 172 (2016) 161–167. doi:10.1016/j.jlumin.2015.11.037.
- [51] P.H. Danielsen, Y. Cao, M. Roursgaard, P. Møller, S. Loft, Endothelial cell activation, oxidative stress and inflammation induced by a panel of metal-based nanomaterials, *Nanotoxicology.* 9 (2015) 813–824. doi:10.3109/17435390.2014.980449.
- [52] N. Yin, Q. Liu, J. Liu, B. He, L. Cui, Z. Li, Z. Yun, G. Qu, S. Liu, Q. Zhou, G. Jiang, Silver Nanoparticle Exposure Attenuates the Viability of Rat Cerebellum Granule Cells through Apoptosis Coupled to Oxidative Stress, *Small.* 9 (2013) 1831–1841. doi:10.1002/sml.201202732.
- [53] P. Carmeliet, Blood vessels and nerves: common signals, pathways and diseases, *Nat. Rev. Genet.* 4 (2003) 710–720. doi:10.1038/nrg1158.
- [54] J. Folkman, Angiogenesis: an organizing principle for drug discovery?, *Nat. Rev. Drug Discov.* 6 (2007) 273–286. doi:10.1038/nrd2115.
- [55] K. Kalishwaralal, S. Sheikpranbabu, S. BarathManiKanth, R. Haribalaganesh, S. RamkumarPandian, S. Gurunathan, Gold nanoparticles inhibit vascular endothelial growth factor-induced angiogenesis and vascular permeability via Src dependent pathway in retinal endothelial cells, *Angiogenesis.* 14 (2011) 29–45. doi:10.1007/s10456-010-9193-x.
- [56] K. Imai, K. Suese, M. Senuma, H. Takashima, Effects of Cell Viability and In Viro Angiogenesis with Nanostructured Zinc Oxide, 3 (2011) 237–241.

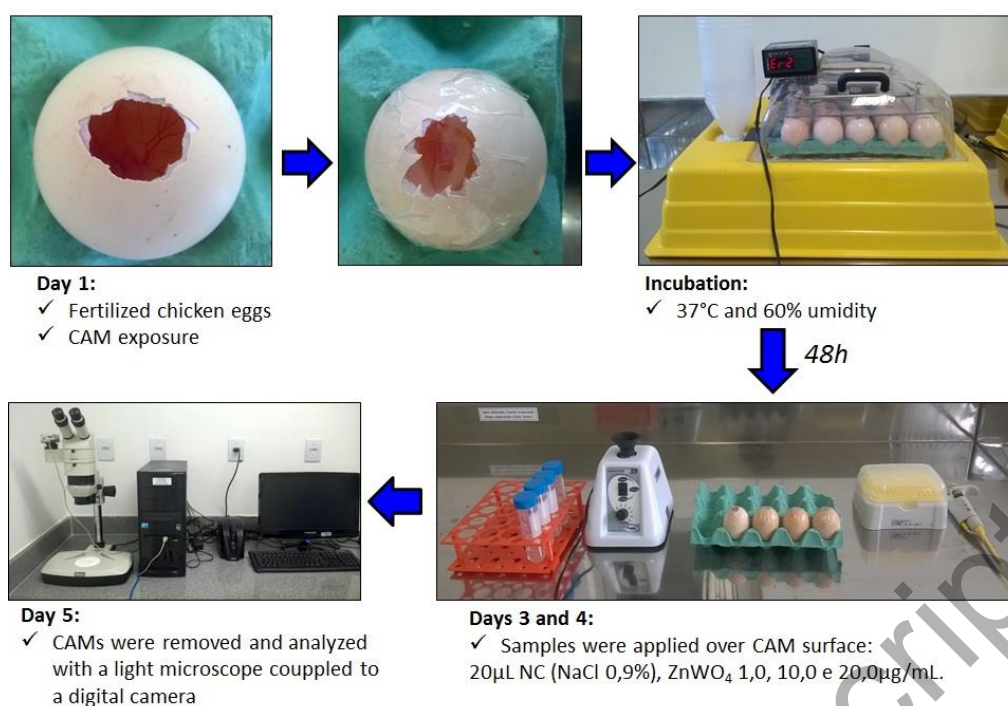


Figure 1- Schematic illustrations of the *in vivo* experimental procedure employed during antiangiogenic activity evaluation. Fertilized chicken eggs were used for the chorioallantoic membrane assay (CAM).



Figure 2– ZnWO₄ nanoparticles obtained with MAHS. A: After being dried. B: Before centrifugation.

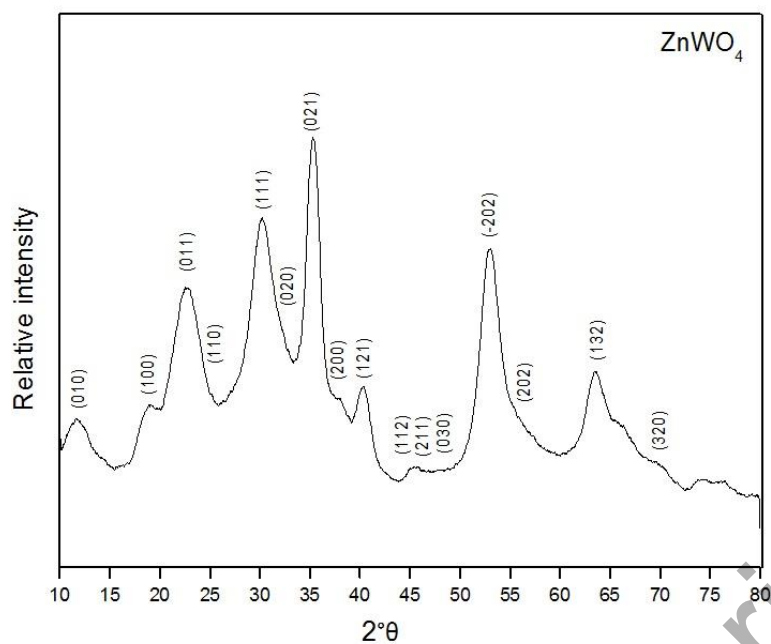


Figure 3- XRD patterns of ZnWO_4 nanoparticles prepared through microwave-assisted hydrothermal synthesis (MAHS) conducted at 120°C , using zinc chloride (ZnCl_2) as the starting precursor.

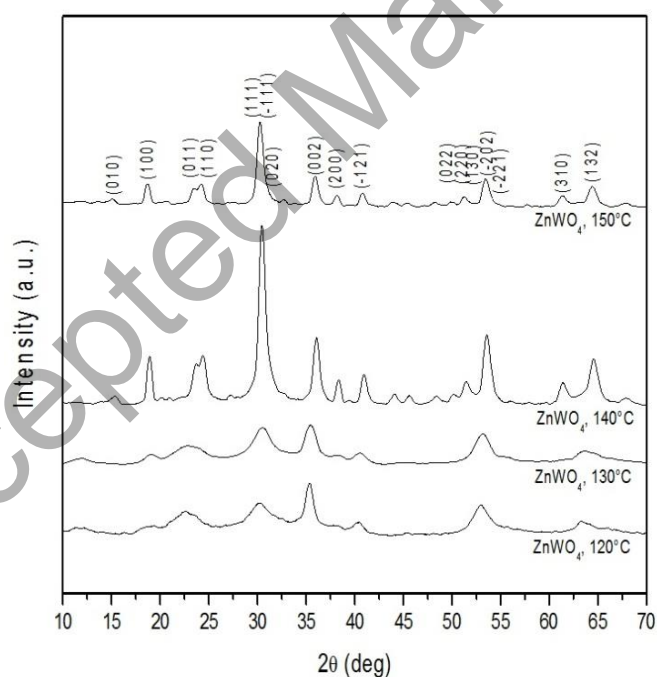


Figure 4- XRD patterns of the ZnWO_4 nanoparticles prepared through microwave-assisted hydrothermal synthesis (MAHS) conducted at 120°C , 130°C , 140°C and 150°C .

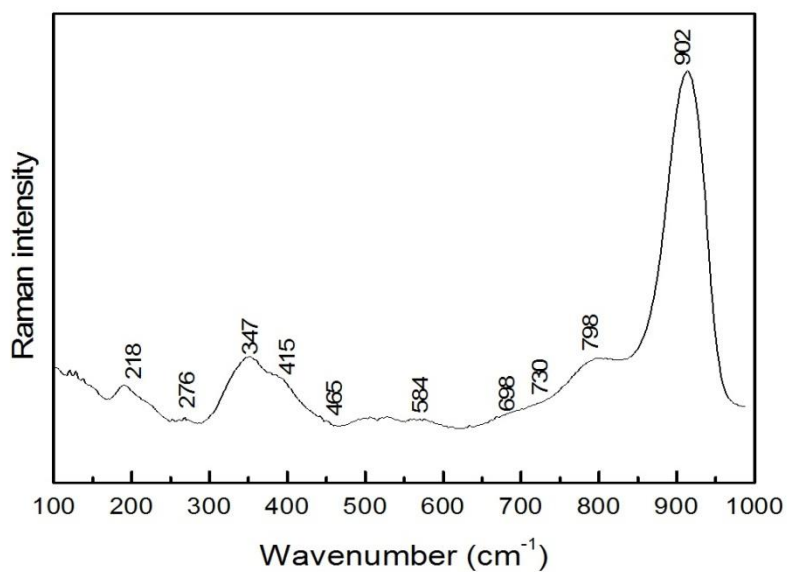


Figure 5. Raman spectra of the ZnWO₄ NPs hydrothermally synthesized at 120°C.

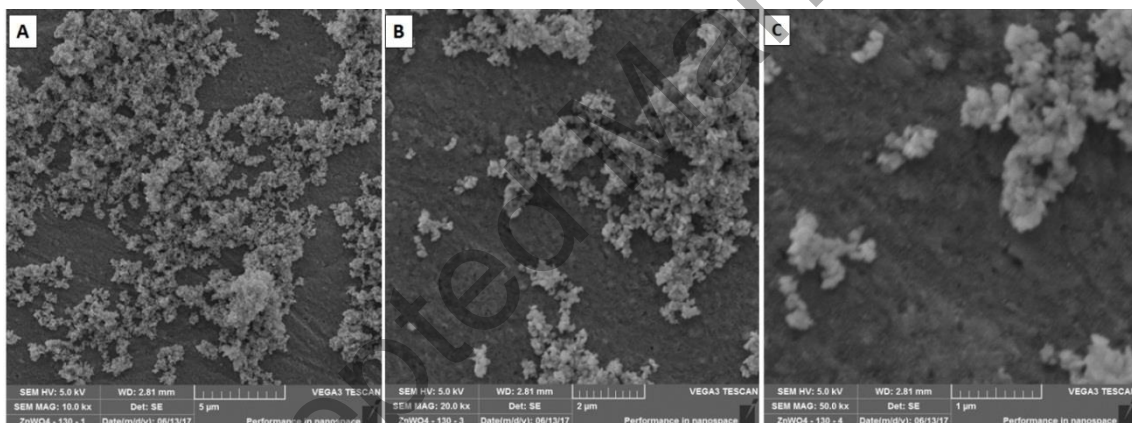
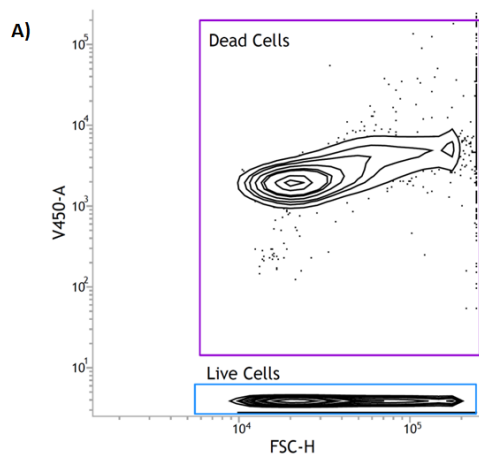
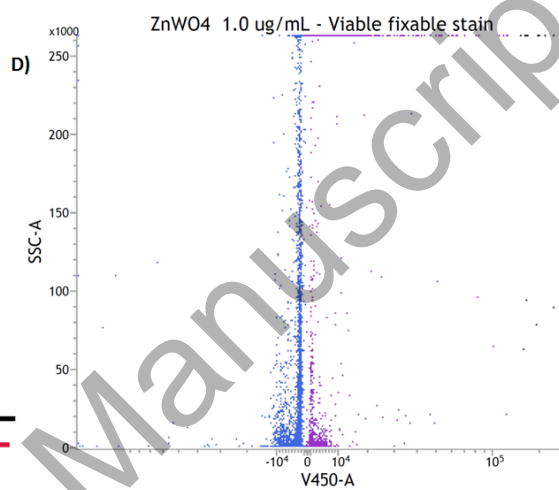
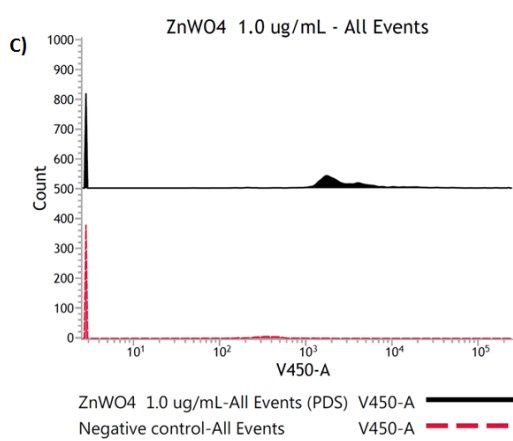


Figure 6. ZnWO₄ nanoparticles SEM images. Magnifications 10.000 X (A); 20.000 X (B); 50.000 X (C).

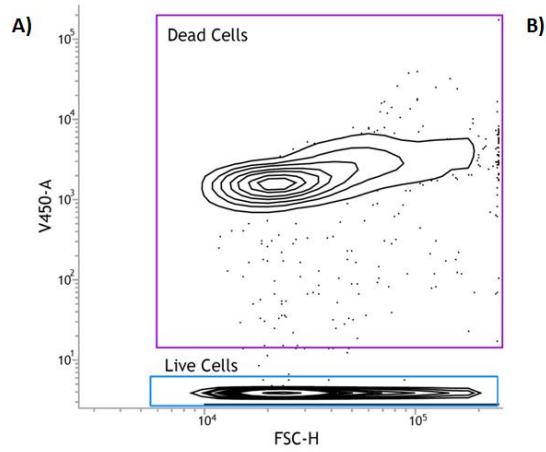


B)

Statistics				
Name	Events	% Parent	% Grandparent	% Total
ZnWO4 1ug/mL:All Events	10,000	***	***	100.00
ZnWO4 1ug/mL:Dead Cells	1,959	19.59	***	19.59
ZnWO4 1ug/mL:Live Cells	7,430	74.30	***	74.30

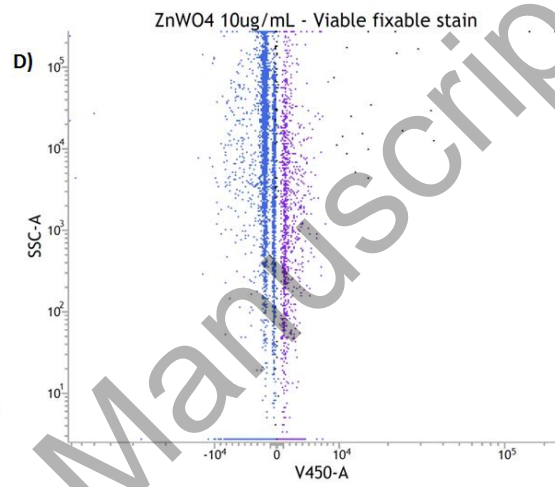
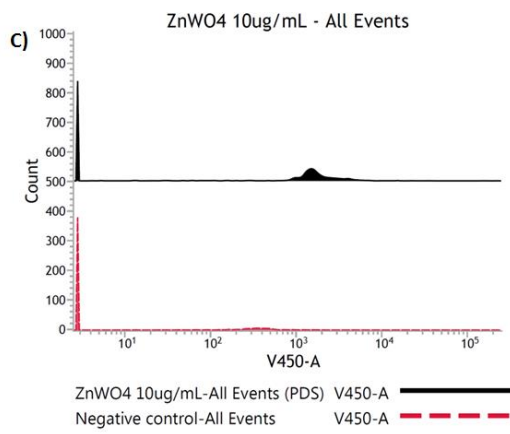


Accepted Manuscript

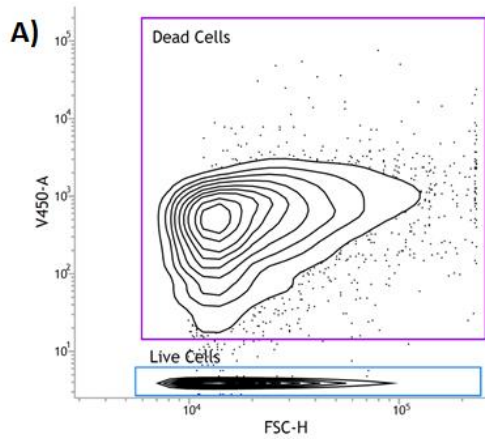


B)

Statistics				
Name	Events	% Parent	% Grandparent	% Total
ZnWO4 10ug/mL:Dead Cells	1,481	14.81	***	14.81
ZnWO4 10ug/mL:Live Cells	8,280	82.80	***	82.80
ZnWO4 10ug/mL:All Events	10,000		***	100.00

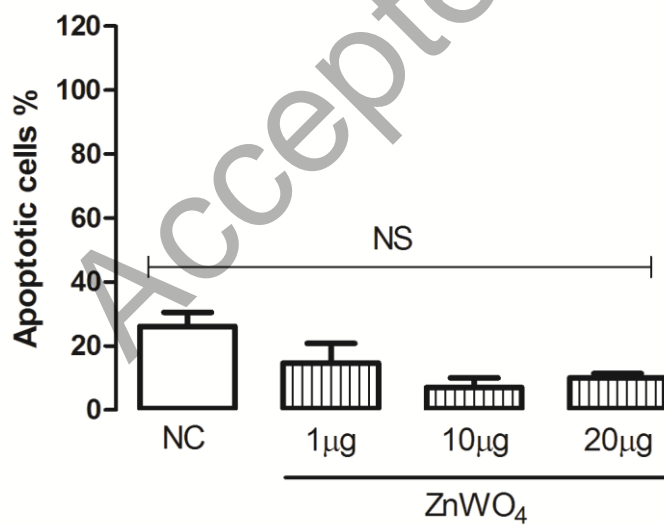
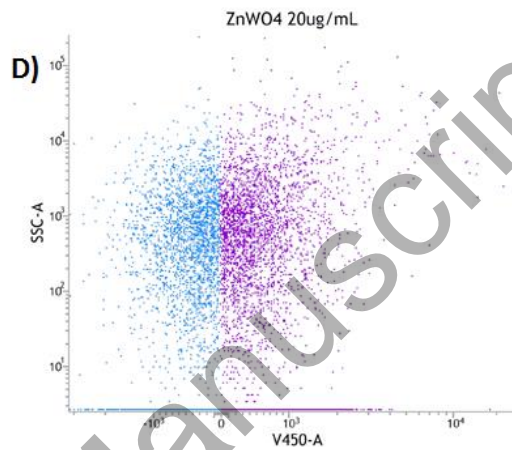
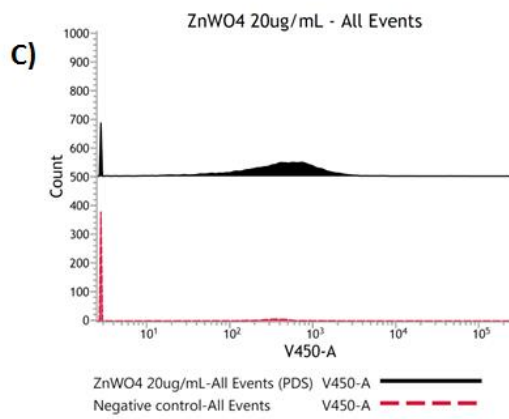


Accepted Manuscript

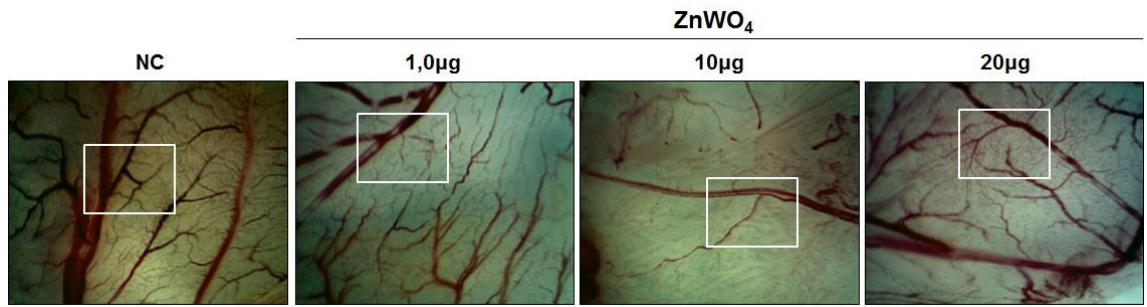


B)

Statistics				
Name	Events	% Parent	% Grandparent	% Total
ZnWO4 20ug/mL:All Events	10,000	***	***	100.00
ZnWO4 20ug/mL:Dead Cells	5,246	52.46	***	52.46
ZnWO4 20ug/mL:Live Cells	4,714	47.14	***	47.14



A



B

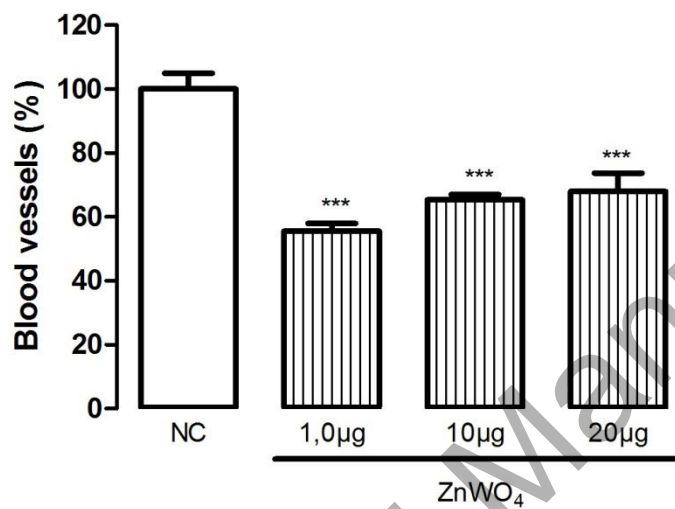


Figure 10. Effects of ZnWO₄ NPs in a CAM model of angiogenesis. The ZnWO₄ induced anti-angiogenic effects. NC: negative control. The values are expressed according to the NC group, which was fixed at 100%. The values are shown as mean ± standard error of the mean (S.E.M.) (n = 5-10/group). ***Values are significantly different from the NC group (p < 0.0001, ANOVA followed by Bonferroni's test).

Table 1 – Average crystallite size for ZnWO₄ nanoparticles obtained by micro-assisted hydrothermal synthesis.

Synthesis temperature (°C)	Average crystallite size (nm)
120	3,67
130	4,68
140	13,25
150	14,42

Table 2. Distribution of mean hydrodynamic diameter for ZnWO₄ obtained by DLS

Mean size (nm)	Distribution of nanoparticle size (%)			
	≤ 200 nm	≤ 300 nm	300 – 500 nm	≥ 500 nm
349.98	1.70	42.20	52.30	3.80

Table 3. Polydispersity index and Zeta potential of ZnWO₄ samples. The analyses were carried out in MilliQ[®] water at 0.9 mg mL⁻¹, pH 7.4. All measurements were performed in triplicate at 25°C.

Samples	Polydispersity index	ζ potential (mV)
ZnWO ₄	0.58 ± 0.17	-17.5 ± 7.07